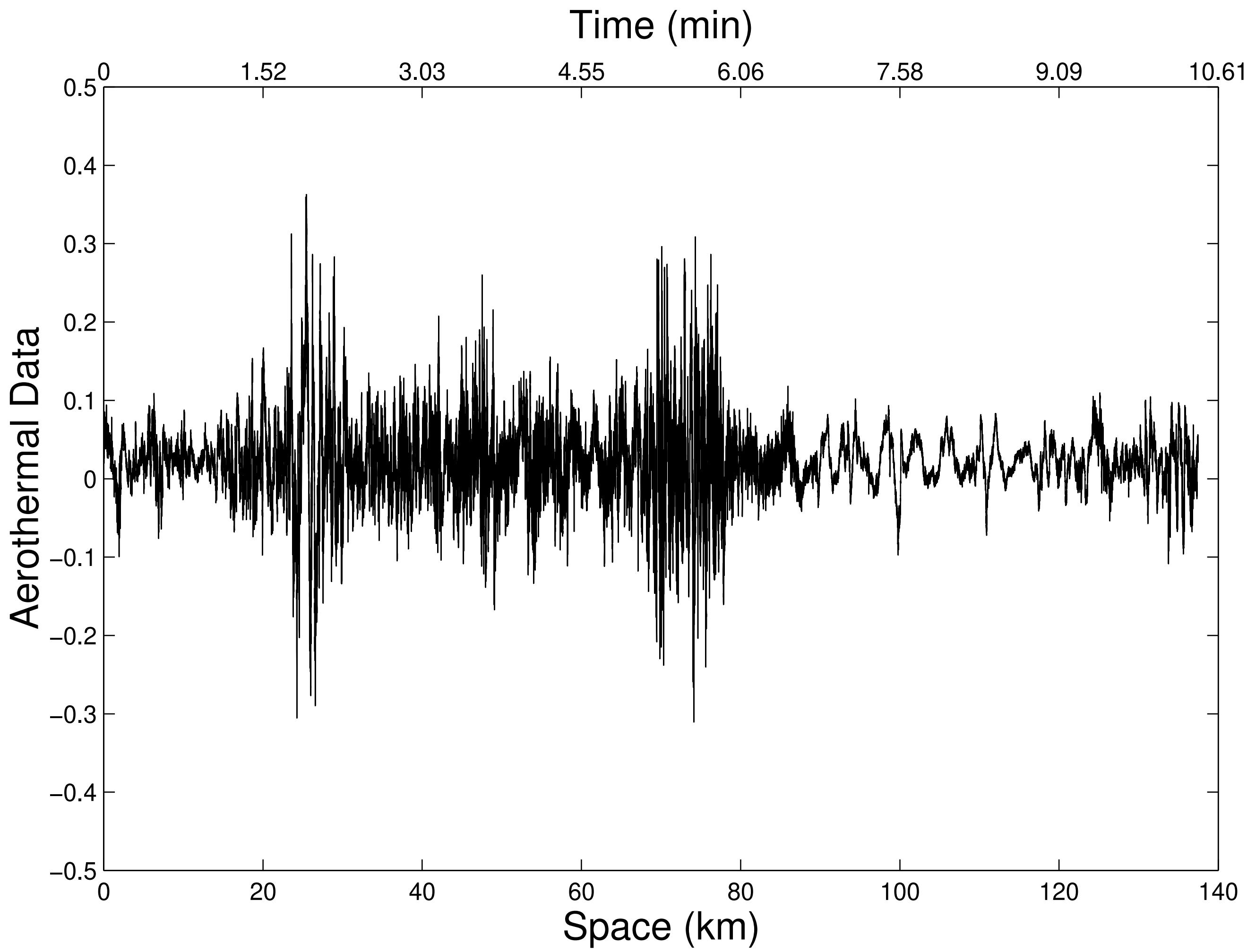

Figure 1. Moving average of aerothermal data over 100 point nonoverlapping blocks.

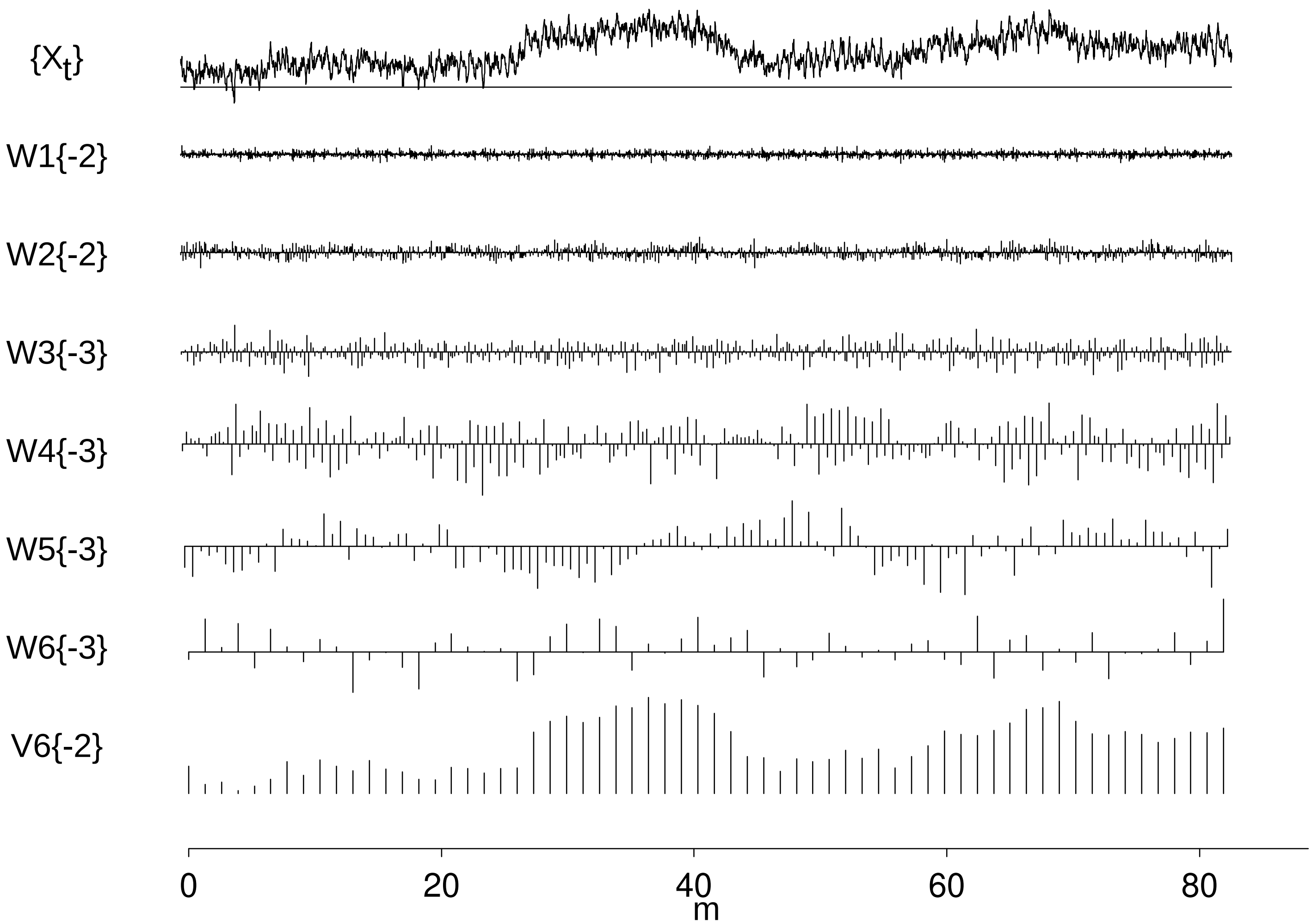

Figure 2. DWT of small segment of aerothermal data. This DWT is based on the LA(8) wavelet filter. The number in the curly brackets next to each subband represents the circular shift imposed to adjust the coefficients so that they are approximately the output from a zero phase filter (a negative value implies an advance, i.e., a circular shift to the left).

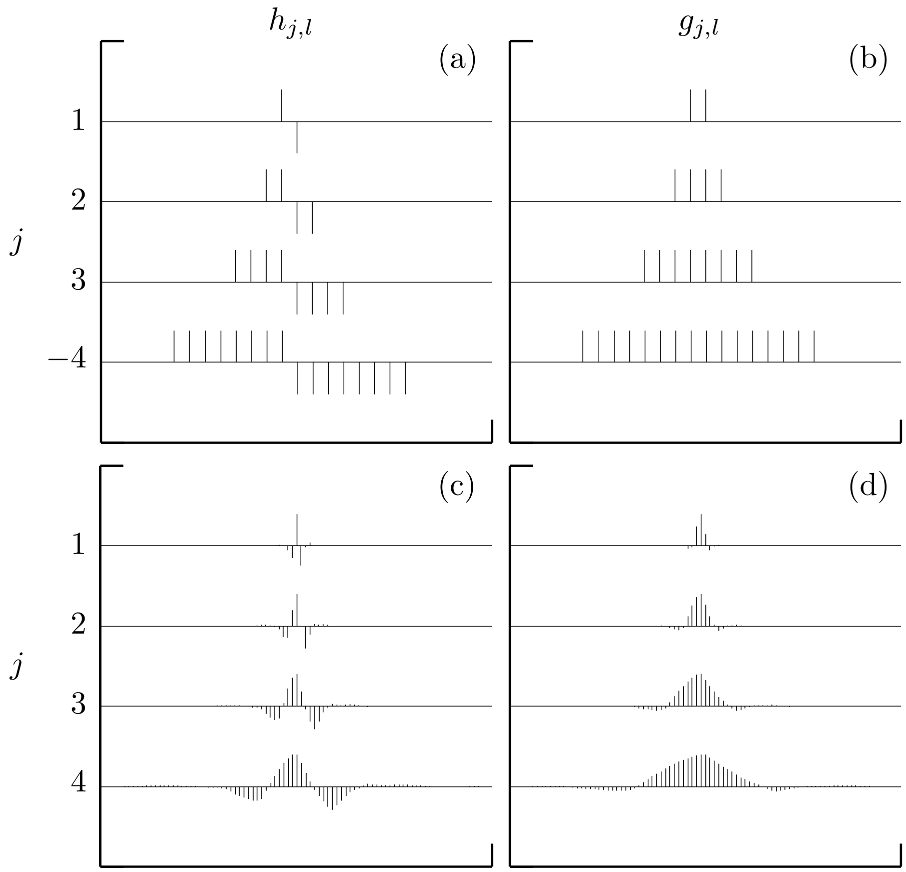

Figure 3. Haar and Daubechies least asymmetric (LA) wavelet and scaling filters. The Haar filters are shown in the top row, and the LA filters, in the bottom. The wavelet filters are shown in the first column, and the scaling filters, in the second column. The LA filters have $L = 8$ nonzero values at level $j = 1$.

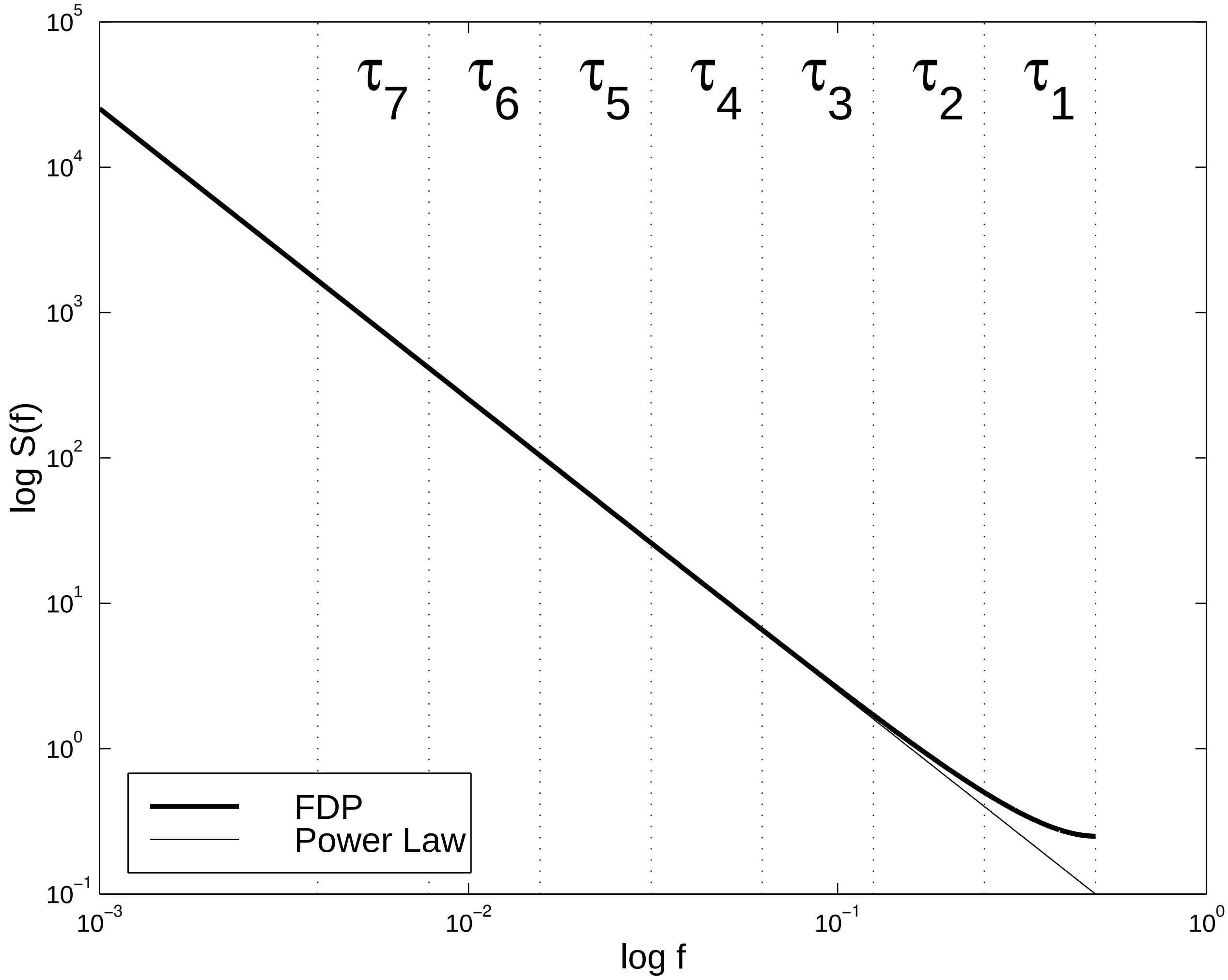

Figure 4. Spectral density function (SDF) for an FD process with $\delta = 1$ (thick curve) compared to that of a pure power law process $|f|^{-2}$ (thin line). The vertical dotted lines delineate the frequency bands corresponding to the scales τ_j for the wavelet coefficients $\mathbf{W}_j$.

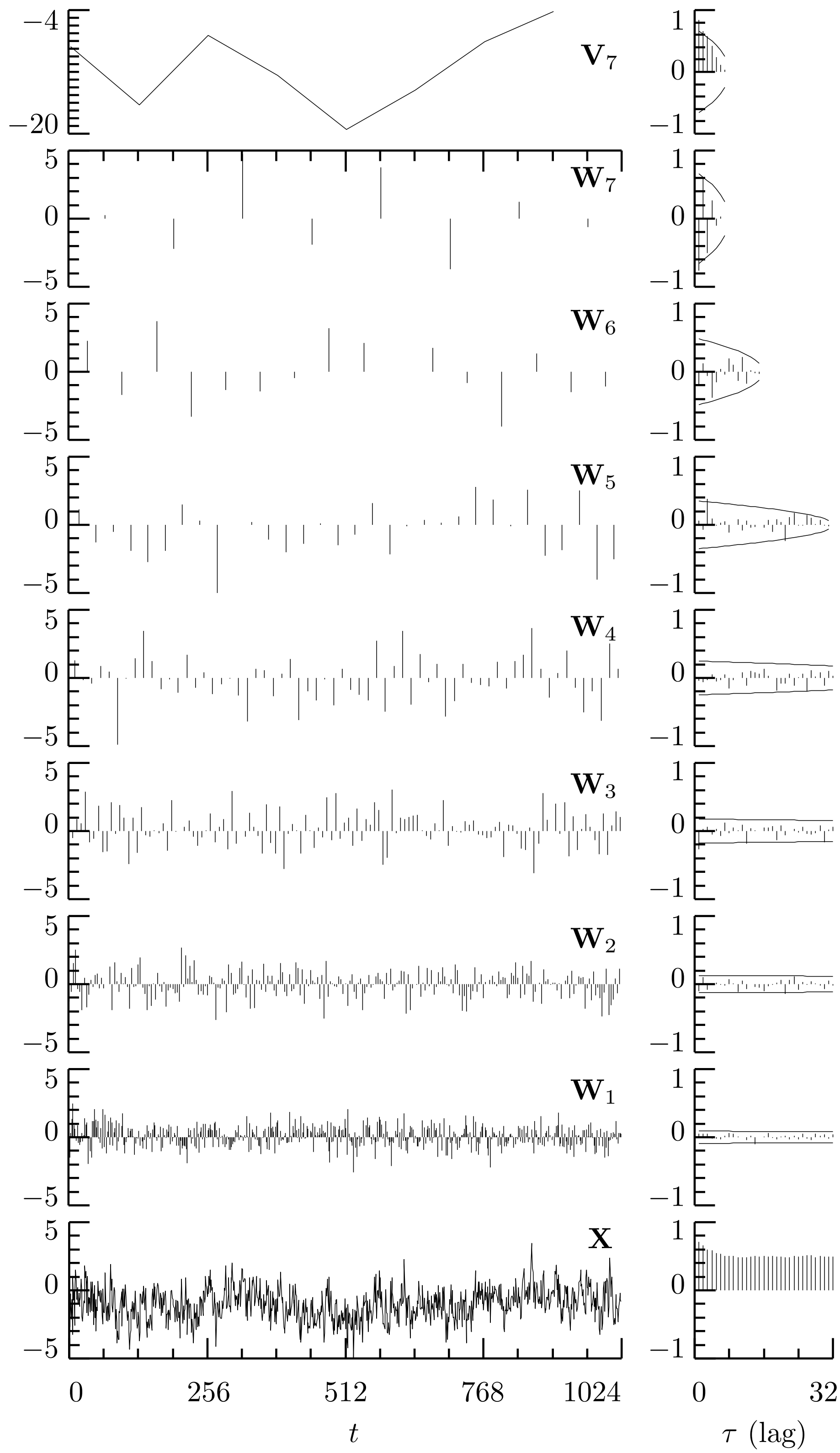

Figure 5. LA(8) DWT coefficients for simulated FD(0.4) time series and sample ACSs.

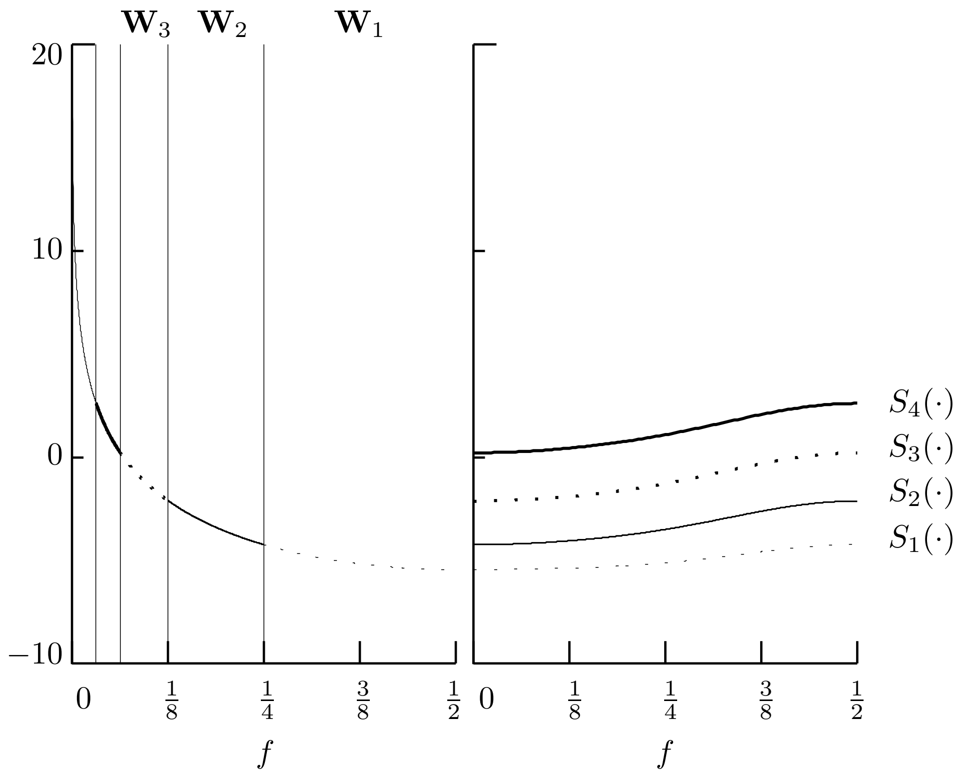

Figure 6. SDFs for an FD(0.4) process (left-hand plot) and for nonboundary LA(8) wavelet coefficients in $\mathbf{W}_1$, $\mathbf{W}_2$, $\mathbf{W}_3$ and $\mathbf{W}_4$ (right-hand). The vertical axis is in units of decibels (i.e., we plot $\log_{10}(S_X(f))$ versus f). The vertical lines in the left-hand plot denote the nominal pass-bands for the four $\mathbf{W}_j$.

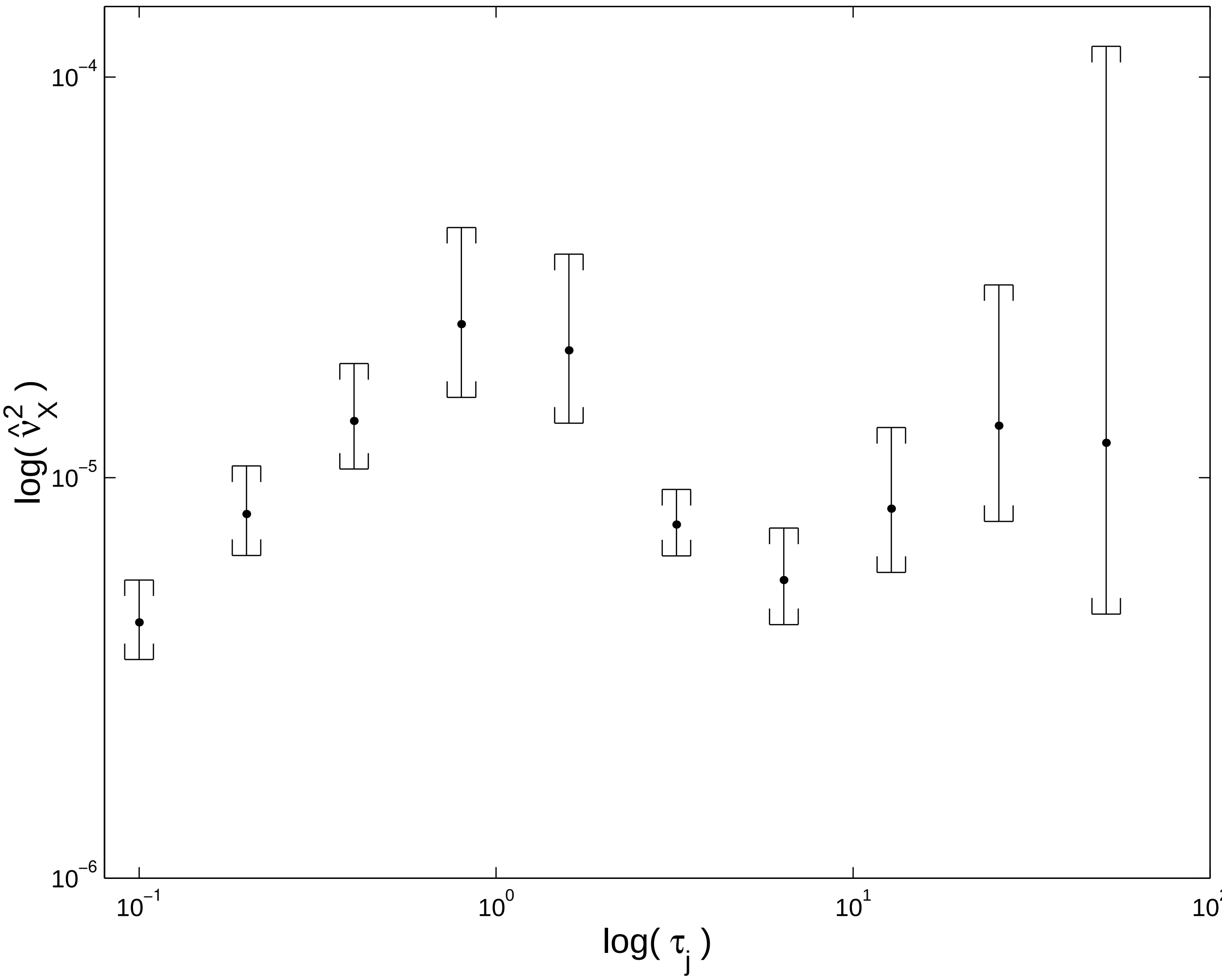

Figure 7. Unbiased MODWT wavelet variance estimator $\hat{\nu}_X^2(\tau_j)$ for one segment of aerothermal data based upon the LA(8) wavelet filter. The confidence intervals are based on a chi-square distribution with the equivalent degrees of freedom being calculated using (i) a large sample approximation to the mean and variance of $\hat{\nu}_X^2(\tau_j)$ for scales $\tau_1, \ldots, \tau_5$ and (ii) an assumption that the spectral density function is flat over the nominal passbands for scales $\tau_6, \ldots, \tau_{10}$.

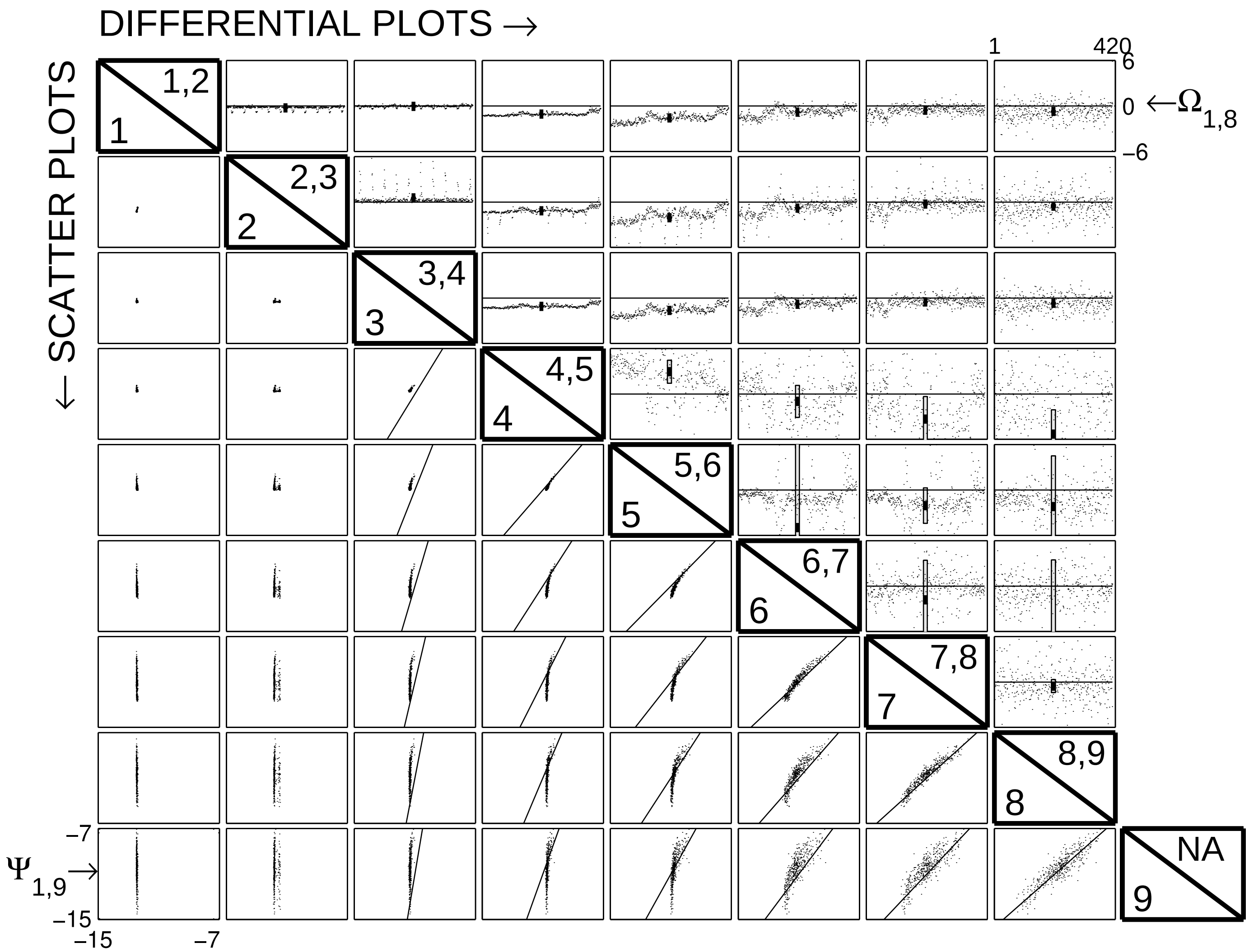

Figure 8. Scatter plots and differential scatter plots of $\log(\hat{\nu}^2_{X,b}(\tau_j))$ estimates for $j = 1, \ldots, 9$ and nonoverlapping blocks b, each containing 10,000 data values.

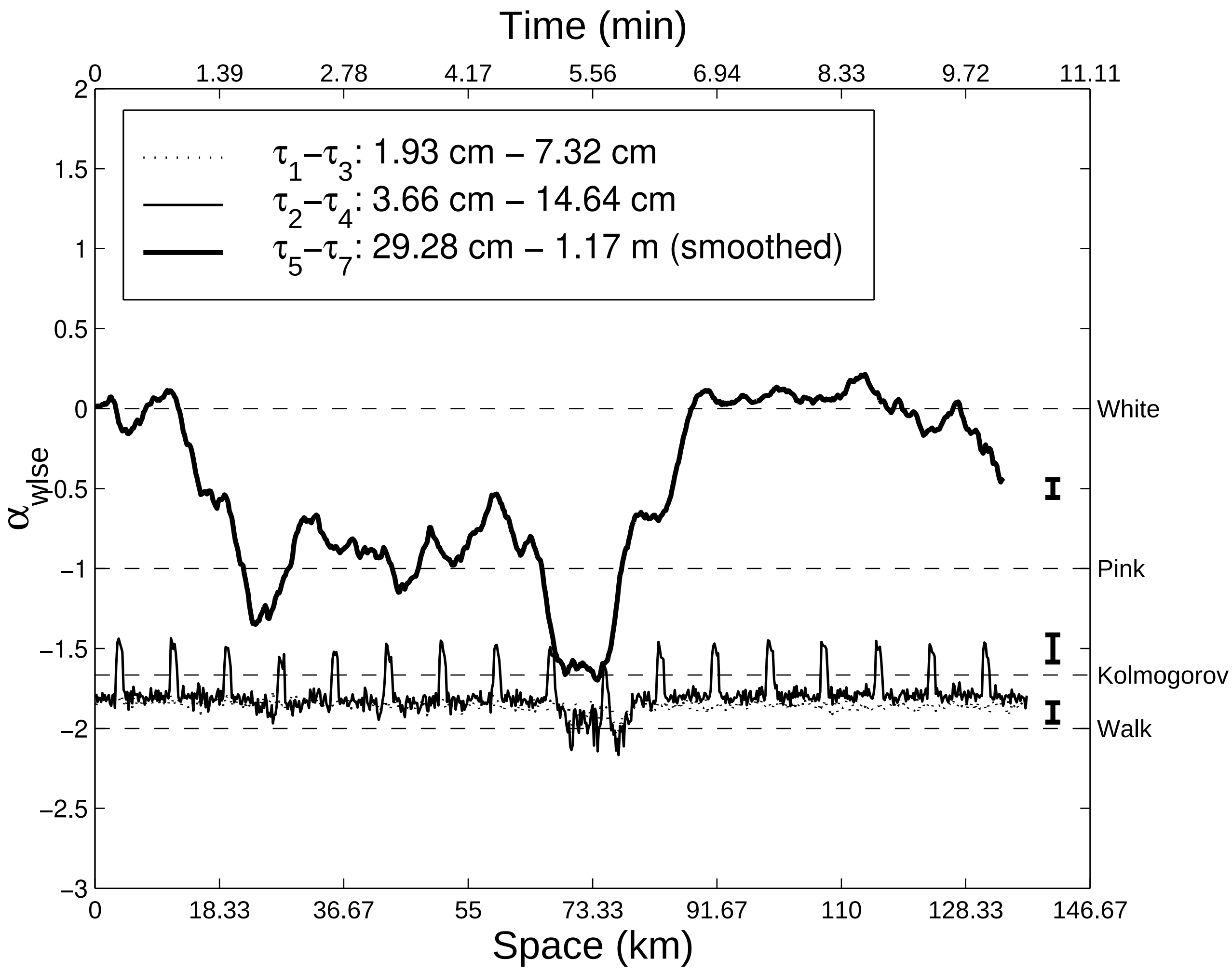

Figure 9. Weighted least squares estimates of the power law exponent $\alpha = -2\delta$ over scales $\tau_1, \ldots, \tau_7$ for the ABL data.

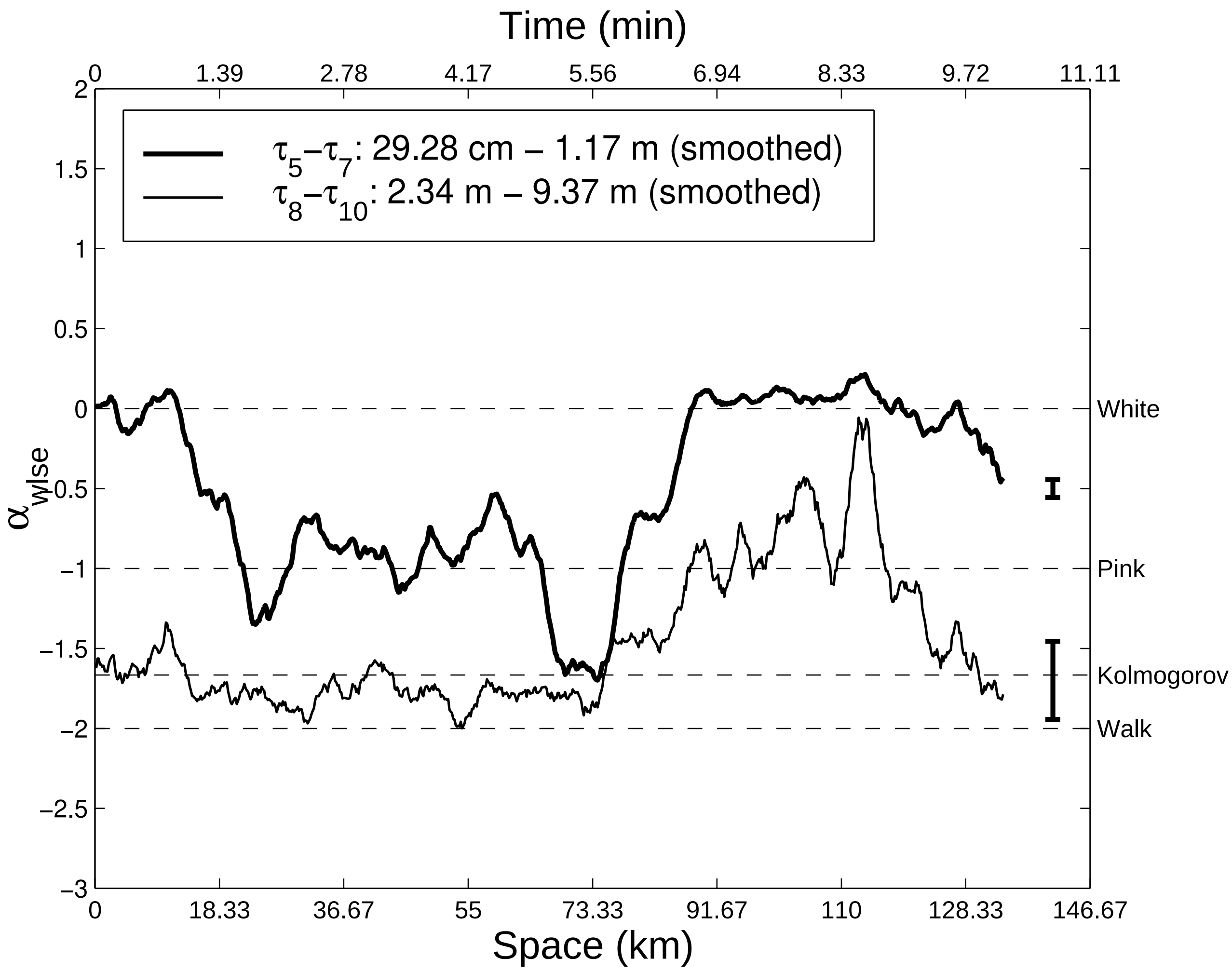

Figure 10. As in Figure 9, but now over scales over scales $\tau_5, \ldots, \tau_{10}$.

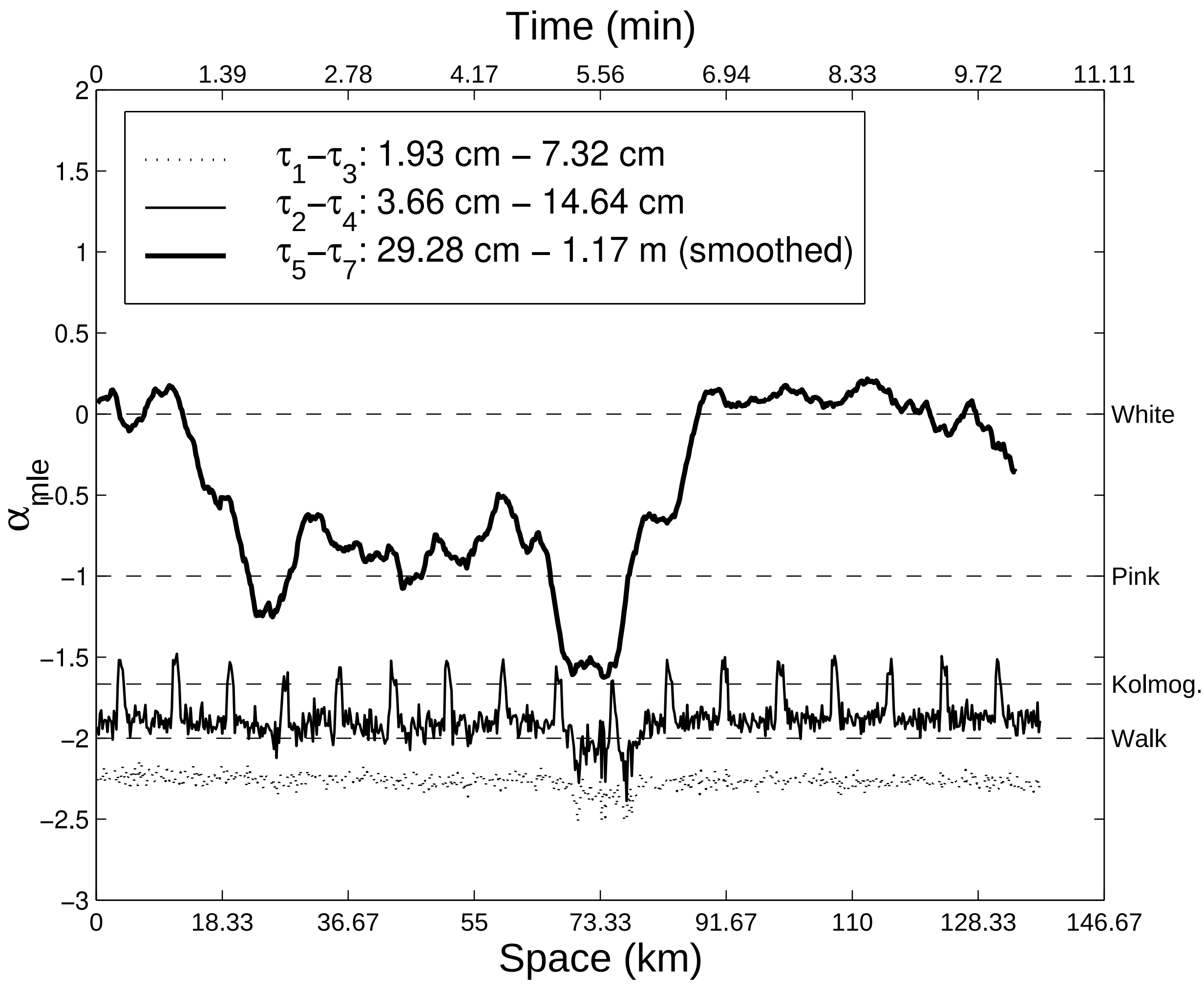

Figure 11. Maximum likelihood estimates of the power law exponent $\alpha = -2\delta$ over scales $\tau_1, \ldots, \tau_7$ for the ABL data.

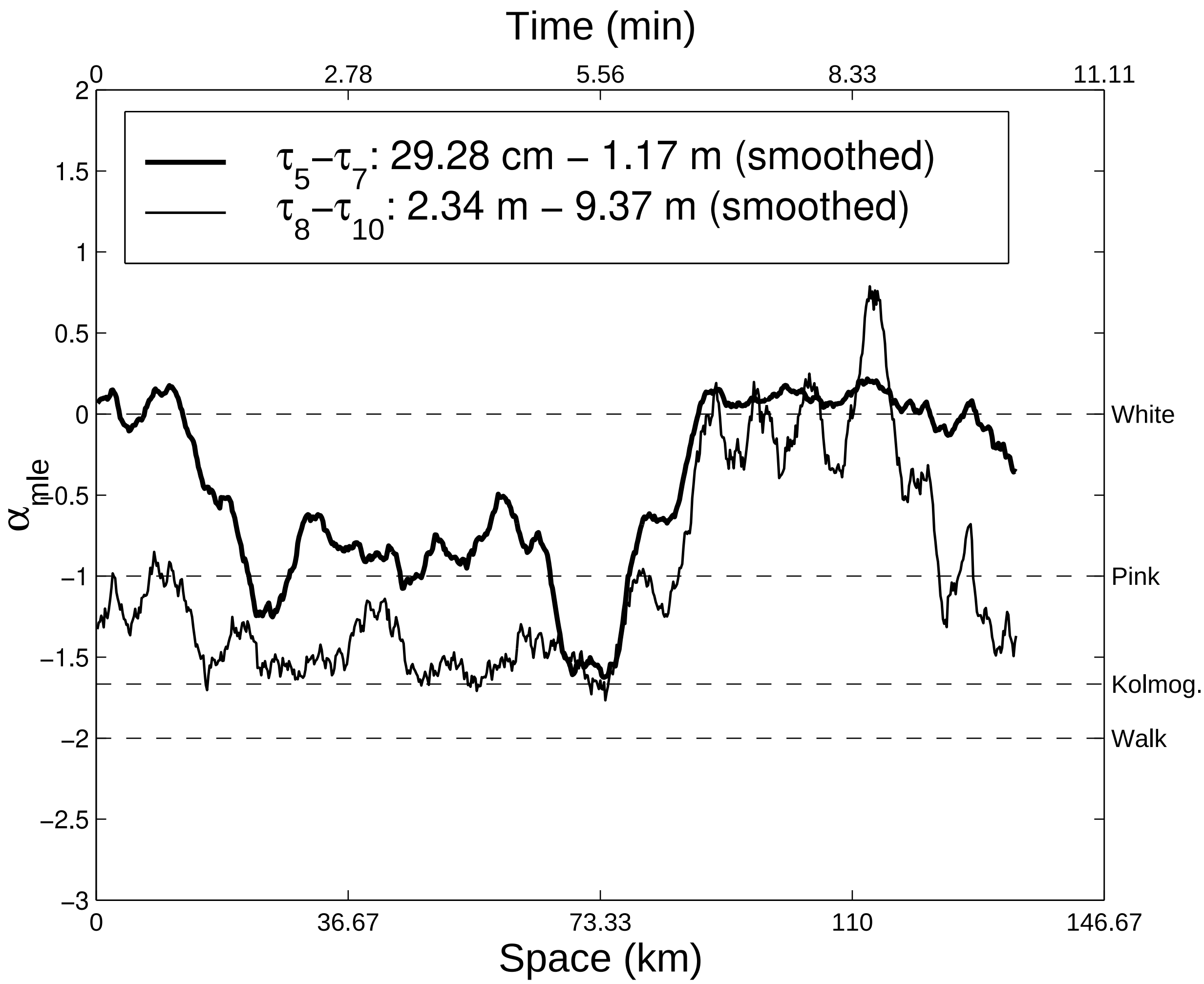

Figure 12. As in Figure 11, but now over scales over scales $\tau_5, \ldots, \tau_{10}$.

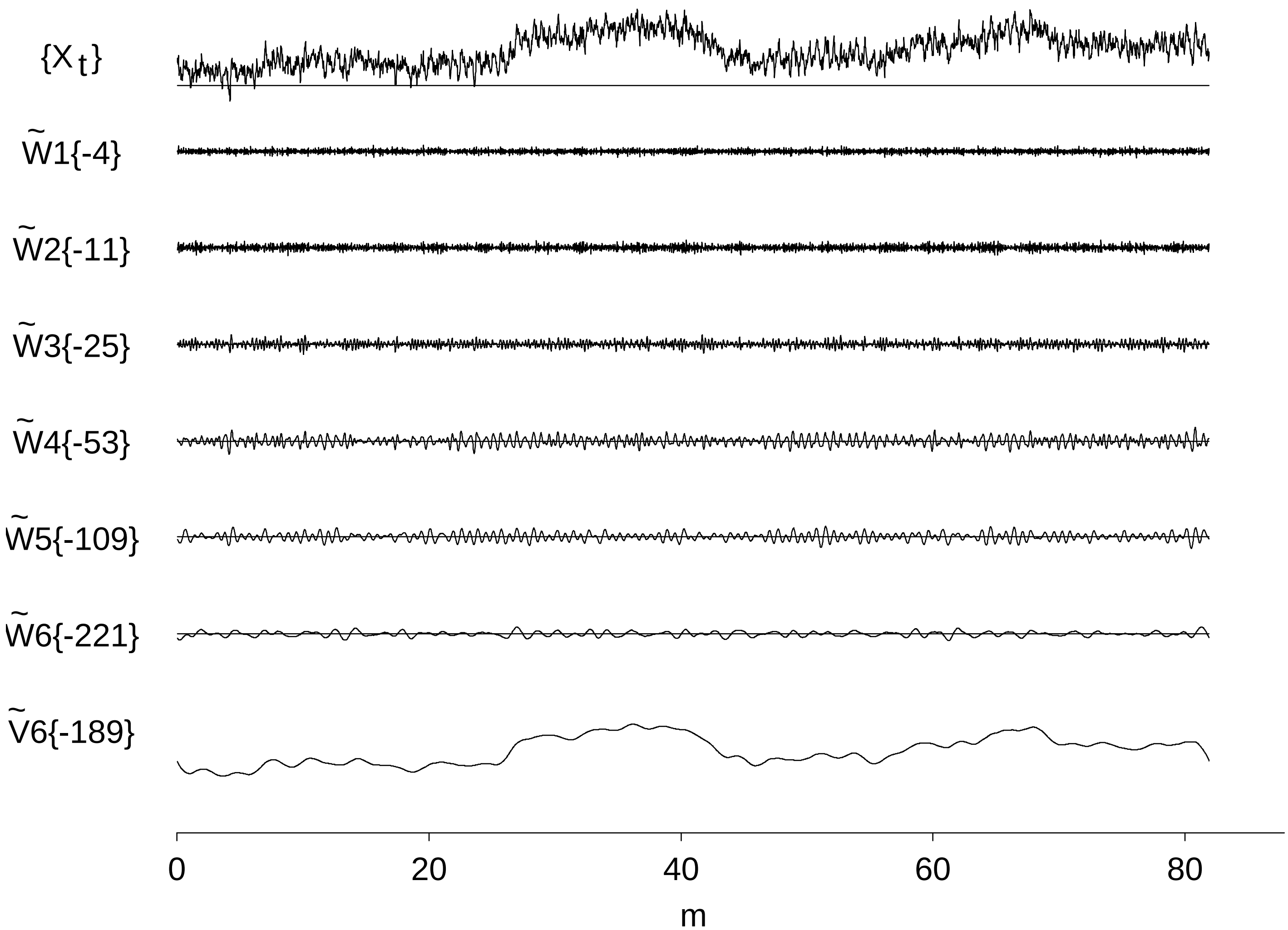

Figure 13. As in Figure 2, but now for the MODWT instead of the DWT.

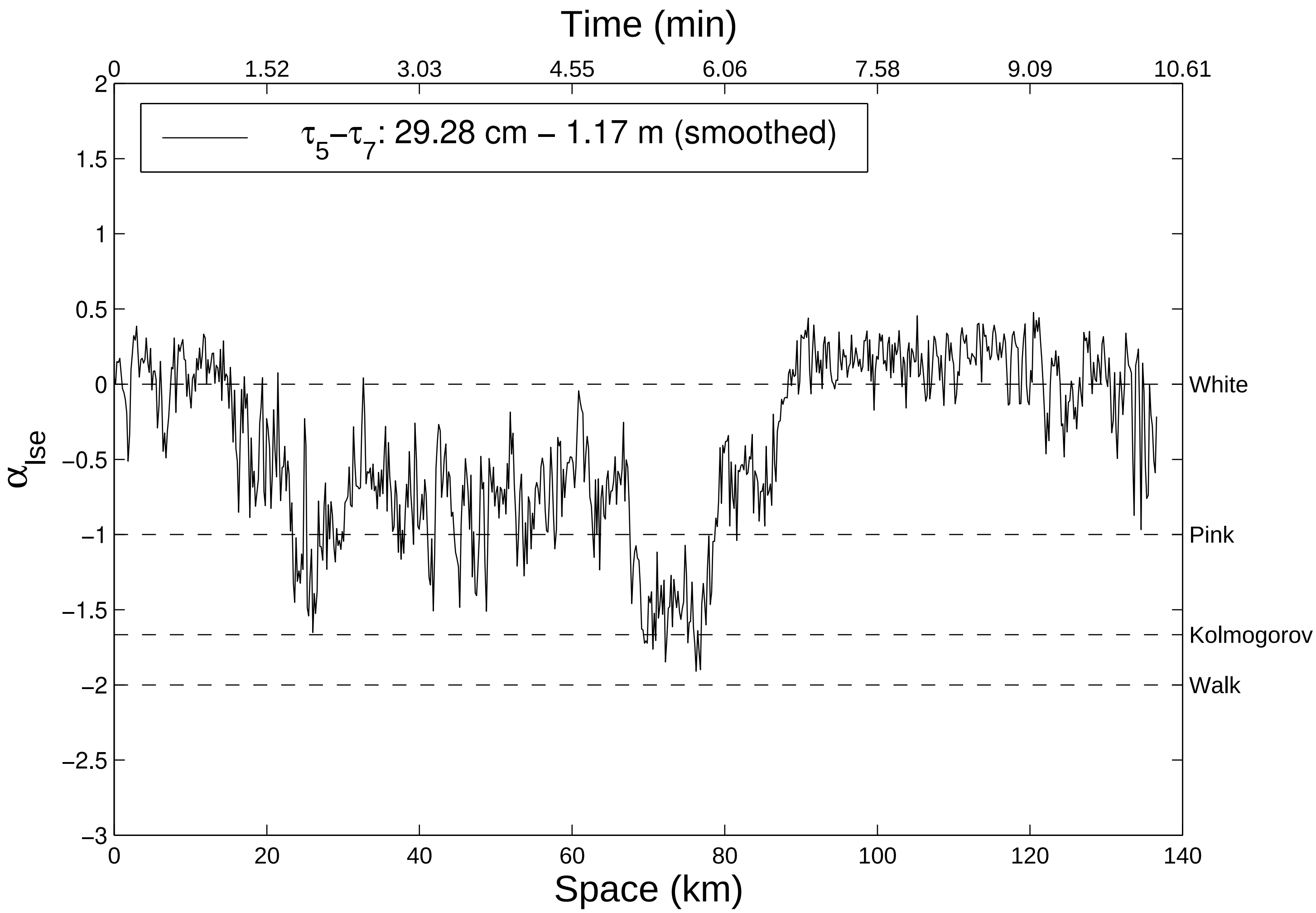

Figure 14. 'Instantaneous' least squares estimates of the power law exponent $\alpha = -2\delta$ over scales τ_5, τ_6 and τ_7 for the ABL data.